Faccioli, et al. Published in Astroparticle Physics, 34(12), 2011: 847-857.

Reducing zero-point systematics in dark energy supernova experiments

L. Faccioli , A.G. Kim , R. Miquel , G. Bernstein , A. Bonissent , M. Brown , W. Carithers , J. Christiansen , N. Connolly , S. Deustua , D. Gerdes , L. Gladney , G. Kushner , E.V. Linder , S. McKee , N. Mostek , H. Shukla , A. Stebbins , C. Stoughton , D. Tucker

A B S T R A C T

We study the effect of filter zero-point uncertainties on future supernova dark energy missions. Fitting for calibration parameters using simultaneous analysis of all Type Ia supernova standard candles achieves a significant improvement over more traditional fit methods. This conclusion is robust under diverse experimental configurations (number of observed supernovae, maximum survey redshift, inclusion of additional systematics). This approach to supernova fitting considerably eases otherwise stringent mission calibration requirements. As an example we simulate a space-based mission based on the proposed JDEM satellite; however the method and conclusions are general and valid for any future supernova dark energy mission, ground or space-based.

Keywords:
Dark energy
Cosmology: observations
Supernovae

1. Introduction

The discovery of the acceleration of the expansion of the universe [23,20] ranks as one of the most significant recent discoveries in cosmology. This acceleration is usually ascribed to a mysterious "dark energy" about which almost nothing is known although there are many competing ideas; what is needed to distinguish between them and shed more light on the nature of the acceleration is more and improved data. Observations of Type Ia supernovae (SNe Ia) have allowed the discovery of the acceleration of the expansion [23,20] and are currently the most established and best understood dark energy probe [1]. The method is described by many authors [19,23,20,21] and is based on the fact that SNe Ia are, to good accuracy, standardizable candles (for a review of SNe Ia as standardizable candles see Phillips [22], Branch and Tammann [5]). However current supernova observations are limited by systematic uncertainties; while this was not a problem when the supernova sample was small and statistical uncertainties were the dominant ones, the growing sample size has already reached the point when statistical and systematic uncertainties are of comparable magnitude, as in e.g. the combined sample of 557 supernovae studied by Amanullah et al. [3] (The Union2 compilation: 2010). As more supernovae will be discovered in the future the need to better characterize and reduce systematic uncertainties will become *the* dominant concern in dark energy experiments. This has been recognized for several years, and the SuperNova/Acceleration Probe (SNAP) satellite[1] (SNAP Collaboration: [25]) was proposed as a systematics-controlled space-based experiment that would put much tighter constraints on dark energy than current and near future experiments by following ≈2000 supernovae out to

z_{max} 1.7. More recently NASA and the Department of Energy have announced the Joint Dark Energy Mission (JDEM)[2,3] as a future space-based mission to study the nature of dark energy by employing a combination of techniques including supernovae. Therefore it is important to characterize the sources of systematics of future supernova experiments; studies of this kind have already appeared [12,13,18,17] and this paper aims at building upon and expanding them.

The two most important sources of systematic uncertainty in dark energy experiments that use supernovae are the dimming by dust in the host galaxy and uncertainties in the flux calibration, specifically the filter zero-points, as seen in recent cosmological analyses such as Astier et al. [4], Wood-Vasey et al. [26], Kowalski et al. [14], Hicken et al. [10], Amanullah et al. [3]. The problem of host-galaxy dimming is also being aggressively pursued, by e.g. targeting supernovae in rich clusters of galaxies [8]; we will include it statistically in our analysis but will not go into its systematics. Properly taking into account zero-point uncertainties is nontrivial because their causes are numerous, ranging from any inaccuracy in the response function of telescope, filter, or detector (from now on collectively indicated as "channel"), or the atmosphere for ground-based experiments, to uncertainties in the calibration procedure. While accurately characterizing all these is obviously an experiment-dependent problem, our aim is to provide a more general way to deal with them.

Starting with a simple model of zero-point uncertainty, we perform a complete end-to-end simulation of a supernova dark energy mission, propagating zero-point uncertainties through the simulation chain, and we evaluate its effects on the final cosmology fit. We do not aim at a detailed physical modeling of particular causes of uncertainty such as imperfect knowledge of the standard stars used to calibrate the zero-points or of the filter response functions, but rather at characterizing their overall effect, whatever their underlying reasons, with a set of zero-points representing the contribution of these important sources of systematics to the final error budget. This will serve as a guide to designers of how much specific components (telescope, filters, detectors, calibration procedure and so on) could be imperfectly known and still achieve the mission objectives.

Our starting point is the result by Kim and Miquel [13, hereafter KM]. KM introduce a new model of filter zero-point uncertainty and show that, due to the standardizable candle nature of SNe Ia, it is possible to treat these uncertainties as parameters that can be included with other parameters in a cosmology analysis. More precisely, KM model the observed peak magnitude m of a supernova as $m = \mu + M + Other + \mathcal{Z}$ where μ is the distance modulus, M is the absolute magnitude after standardization (and therefore the same for all supernovae), "*Other*" indicates all residual effects that influence m, such as host galaxy extinction, and $\mathcal{Z}$ is a new fit parameter for zero-point offsets to be fit with all the other parameters in the model. It is important to note that modeling zero-point offsets as fit parameters would not be possible if SNe Ia were not standardizable candles because M would not be the same for every supernova. KM show that by fitting for all the supernovae distance moduli *simultaneously* it is possible to achieve a significant reduction in the final uncertainties in the cosmological parameters with respect to the traditional case when supernova distances are fit one by one and calibration uncertainties are then included in the total error budget. In the rest of the paper we will refer to the KM fitting approach as "simultaneous fit" and to the traditional approach as "SN by SN fit".

This work expands KM in several ways:

1. KM carry out a Fisher matrix analysis of their model; we perform a complete end-to-end simulation of a supernova dark energy mission, with a realistic modeling of all its aspects.
2. KM use a particular z distribution, in which all supernovae are placed at those special redshifts that have zero K-correction. At those z the improvement in mission performance is maximum; we study a more realistic z distribution.
3. We include an intrinsic color dispersion.
4. We investigate whether our conclusions are robust with respect to several changes in mission parameters (number of supernovae, maximum redshift, inclusion of additional systematics); our simulation tool allows us to explore a much wider parameter space than KM.

It is important to point out that the KM model that we adopt here is applicable to a generic future dark energy mission based on supernovae; however, for concreteness we will present our results by considering a specific example: the supernova survey of the future space-based dark energy mission based on the proposed SNAP satellite. We will also assume that a nearby sample of supernovae, whose characteristics are based on the expected Nearby Supernova Factory sample[4] [2,7], is available: specifically this sample is comprised of 316 supernovae with $0.03 \leqslant z \leqslant 0.08$.

The paper is organized as follows: Section 2 describes the KM model and its implementation in our simulation tool, Sections 3 and 4 describe our results and Section 5 summarizes our conclusions and discusses ways the work can be expanded. In what follows we will use the terms "mission" and "experiment" interchangeably.

2. Supernova model and implementation

Our analysis begins with a set of supernova statistics (peak magnitudes and stretches) in different bands, representing both the distant sample that our simulated mission will observe and the nearby sample that we assume already available; these statistics are obtained in the following way. For each supernova a redshift is chosen from a specified redshift distribution and fluxes and their uncertainties are computed by convolving spectral templates from [11] with the channel throughputs; this results in a set of simulated supernova fluxes in different bands at different epochs. The flux variability due to Poisson noise is simulated by drawing the fluxes from a Gaussian distribution, which is appropriate in the limit of high expected numbers of photons. Each band is then fit independently of the others, following Hsiao et al. [20], to give, among other parameters, an estimated flux at maximum and a stretch in each band; the covariance matrix is also computed and propagated later. Up to and including the stage of light curve fitting, the two approaches, simultaneous fit and SN by SN fit, do not differ and they are carried out in the same way by our analysis. We then fit for the distance moduli (hereafter "μ fit"); this is the step where the differences in the two approaches are manifest, and we describe the models we used for each approach in more detail in the next two subsections. We then describe the data error model used both by the μ fit and the cosmology fit, the cosmology fit itself, which again is performed in the same way for simultaneous fit and SN by SN fit, and finally the mission parameters we use. In the rest of the paper N_{SN} will denote the number of supernovae observed by the mission, excluding the nearby sample and $N = N_{SN} + N_{Nearby}$ will denote the total number of observed supernovae.

[2] http://jdem.gsfc.nasa.gov/.
[3] http://jdem.lbl.gov/.
[4] http://snfactory.lbl.gov/.

2.1. Simulating the zero-point uncertainty in the SN by SN fit: a Monte Carlo approach

In this section we present how the SN by SN analysis is performed. After converting fitted peak fluxes to magnitudes we model these and the stretches as:

$$\begin{aligned} m_k^i &= \mu^i + \alpha(S^i - 1) + M(z_i)_k + A_V^i a(z_i)_k + B_V^i b(z_i)_k, \\ s_k^i &= S^i, \end{aligned} \tag{1}$$

with $i = 1,\ldots,N$; for each supernova i ,k belongs to the subset of $\{1,\ldots,N_F\}$ that covers restframe optical and near infra-red (NIR) wavelengths and N_F denotes the number of filters used in the mission; in our simulations we assume $N_F = 8$. The meaning of the symbols in Eqs. (1) is as follows, distinguishing between *input data*, *model parameters*, and *known functions*.

1. *Input data from simulations:*
   (a) m_k^i denotes the simulated peak instrumental magnitudes of supernova i in observer frame band k obtained after light curve fitting.
   (b) s_k^i denotes the stretch of supernova i in observer frame band k after light curve fitting.
2. *Model parameters:*
   (a) μ^i denotes the distance modulus of supernova i.
   (b) S^i is a weighted stretch parameter for supernova i used to fit for μ^i; unlike s_k^i which depends on the observer frame band, there is a single parameter S^i for each supernova.
   (c) A_V^i and $B_V^i \equiv (A_V/R_V)^i$ are extinction parameters (CCM: [6]).
3. *Known functions:*
   (a) $M(z_i)_k$ is the absolute peak magnitude of a $S = 1$ supernova at redshift z_i in observer frame band k, given by:

$$M(z_i)_k = -2.5\log\left(\int \mathrm{d}\lambda f((1+z_i)\lambda)T_k(\lambda)\right), \tag{2}$$

   where $f(\lambda)$ is a template spectrum from Hsiao et al. [11] and $T_k(\lambda)$ is the throughput of channel k, with λ the observer frame wavelength.
   (b) $a(z_i)_k$ and $b(z_i)_k$ model host galaxy extinction and are computed in a manner similar to $M(z_i)_k$:

$$\begin{aligned} a(z_i)_k &= -2.5\log\left(\int \mathrm{d}\lambda a_{\mathrm{CCM}}((1+z_i)\lambda)f((1+z_i)\lambda)T_k(\lambda)\right), \\ b(z_i)_k &= -2.5\log\left(\int \mathrm{d}\lambda b_{\mathrm{CCM}}((1+z_i)\lambda)f((1+z_i)\lambda)T_k(\lambda)\right), \end{aligned} \tag{3}$$

   where $a_{\mathrm{CCM}}(\lambda)$ and $b_{\mathrm{CCM}}(\lambda)$ are known functions of wavelength, describing host galaxy extinction; we assume a CCM extinction law.
   (c) α is a fixed dimensionless constant; we assume $\alpha = -1.7$.

For each supernova $i = 1,\ldots,N$ we fit for μ, S, A_V, and B_V.

Our chosen value for α was based on older values and is somewhat larger, in absolute value, than those found by recent analyses of supernova data: for example Kowalski et al. [14] find $\alpha = -1.46 \pm 0.16$ (note that with our sign convention in Eqs. (1) ($\alpha < 0$) for the supernovae in the $z > 0.2$ Union subsample, which is the relevant one since in our subsequent analyses we will assume $z > 0.3$. This may result in a conservative parameter estimation in all our simulations but would not change our conclusions.

We now include zero-point uncertainties, which are not described in the system of Eqs. (1). The usual approach to incorporating zero-point uncertainties is to estimate them and include them in the total error budget (see Amanullah et al. [3] for an attempt at jointly modeling zero-point uncertainties and other systematics taking their covariances into account). Following KM we implement the usual approach by modeling the zero-point uncertainty in each bandpass k via a peak magnitude shift, described by a parameter $\mathcal{Z}_k$, for supernova i in observer frame band k.

$$m_k^i \to m_k^i + \mathcal{Z}_k, \quad \forall i \tag{4}$$

where $\mathcal{Z}_k$ is a random shift drawn from a Gaussian distribution with 0 mag mean; the value of its standard deviation quantifies our prior knowledge of the filter zero point uncertainty, $\sigma_{\mathcal{Z}}$. Since the light curve fitter fits for a peak flux, $f_{0k} = 10^{-0.4m_k(max)}$, the magnitude shift is actually converted to flux before being applied, according to the usual expression:

$$f_{0k} \to f_{0k} \times 10^{-0.4\mathcal{Z}_k}. \tag{5}$$

The same magnitude shift $\mathcal{Z}_k$ affects all supernovae that are observed through filter k; since this band in the restframe varies from supernova to supernova depending on their redshifts, the same $\mathcal{Z}_k$ affects different supernovae in different ways, introducing a *correlation* between their distance moduli μ. Neglecting for the moment other sources of variability, for supernova i we may write: $\mu^i = m_k^i - M(z_i)_k$, where $M(z_i)_k$ is defined in Eq. (2). Then as $m_k^i \to m_k^i + \mathcal{Z}_k \Rightarrow \mu^i \to \mu^i + \mathcal{Z}_k$; the μs become correlated via the $\mathcal{Z}_k$ parameters and their covariance matrix becomes non-diagonal.

The contribution of the filter zero-point uncertainty to the overall μ covariance matrix is estimated via a Monte Carlo approach (MC): at each MC realization a different set of magnitude shifts $\mathcal{Z}_k$, one for each filter, is drawn from a Gaussian distribution with 0 mag mean and a chosen standard deviation; we run the MC with standard deviations ranging from 0.001 mag to 0.05 mag; each MC run is iterated 500 times.

In principle the MC should be run on the actual data sample; however for simplicity we chose to run the MC on a smaller sample of supernovae, to derive a μ covariance matrix for this smaller dateset, and to calculate the μ covariance matrix for the larger dataset by interpolating the matrix computed for the smaller one.

More specifically we proceed as follows:

1. Generate a set of supernovae, labeled by a, at redshifts s $z_a = 0.01,\ldots,1.7$ in increments of 0.01; each supernova has a stretch $S = 1$ and no extinction so that the only source of variation in the dataset is the one introduced by the filter zero-point uncertainty.
2. Fit the light curves of these supernovae and obtain the flux at maximum f_{0k} in filter k.
3. Run the MC: at each realization v a different set of magnitude shifts $\mathcal{Z}_k$ is generated, converted to flux, and applied to f_{0k} as in Eq. (5).
4. Fit for the distance moduli μ_v^a at each realization v; repeat steps 3 and 4 for 500 realizations.
5. At the end of the MC, compute a μ covariance matrix in the usual way: for a pair of supernovae denoted by a, b:

$$(V_{\mathrm{ZP}})_{ab} = \langle \mu^a \mu^b \rangle - \langle \mu^a \rangle \langle \mu^b \rangle, \tag{6}$$

   where

$$\begin{aligned} \langle \mu^a \mu^b \rangle &= \frac{1}{N_{\mathrm{NR}}} \sum_{v=1}^{N_{\mathrm{NR}}} \mu_v^a \mu_v^b, \\ \langle \mu^a \rangle &= \frac{1}{N_{\mathrm{NR}}} \sum_{v=1}^{N_{\mathrm{NR}}} \mu_v^a \end{aligned} \tag{7}$$

   and $N_{\mathrm{NR}} = 500$.

The covariance matrices thus computed are stored for use with the full dataset. For each pair of supernovae i, j, at redshifts z_i, z_j, in the full dataset, an entry of $(V_{\mathrm{ZP}})_{ij}$ is computed by spline interpolat-

ing the matrix defined in Eq. (6) between redshifts s z_a, z_b and z_{a+1}, z_{b+1} with $z_a \leqslant z_i \leqslant z_{a+1}$ and $z_b \leqslant z_j \leqslant z_{b+1}$; this matrix is added to the statistical μ covariance matrix, V_μ and to any other covariance matrix describing some systematic, $V_{\rm Sys}$, such as the systematic model described in Linder and Huterer [15].

Fig. 1 shows, in the upper panel, the square root of the diagonal elements of the covariance matrix computed via Eqs. (7), $\sigma_a \equiv \sqrt{\langle(\mu^a)^2\rangle - \langle\mu^a\rangle^2}$, for different values of the zero-point prior $\sigma_{\mathcal{Z}}$. The high values of these elements compared with the values of the prior, especially at high z (e.g.: σ_a 0.5 mag at z 1.6 for $\sigma_{\mathcal{Z}} = 0.05$ mag) is explained by the dust model we adopted: a CCM model in which we fit both for A_V and for $B_V \equiv A_V/R_V$. As an alternative one could fix R_V and fit only for A_V when running the MC; we tried this as well, fixing $R_V = 3.1$, and obtaining values of σ_a a factor of 3.5 lower than those obtained when fitting for B_V; these results are shown in the lower panel of Fig. 1, plotted on the same scale as the upper panel to show the difference. In the results we report later for the SN by SN fit we always use covariance matrices obtained by fitting B_V in the MC. In both cases the curves are roughly proportional to each other by the ratio of their zero-point priors. Fig. 2 shows color maps of a few covariance matrices computed via the MC: the upper left panel shows the matrix corresponding to a zero-point prior of 0.005 mag, the upper right to a prior of 0.01 mag, the lower left to a prior of 0.02 mag, and the lower right to a prior of 0.05 mag.

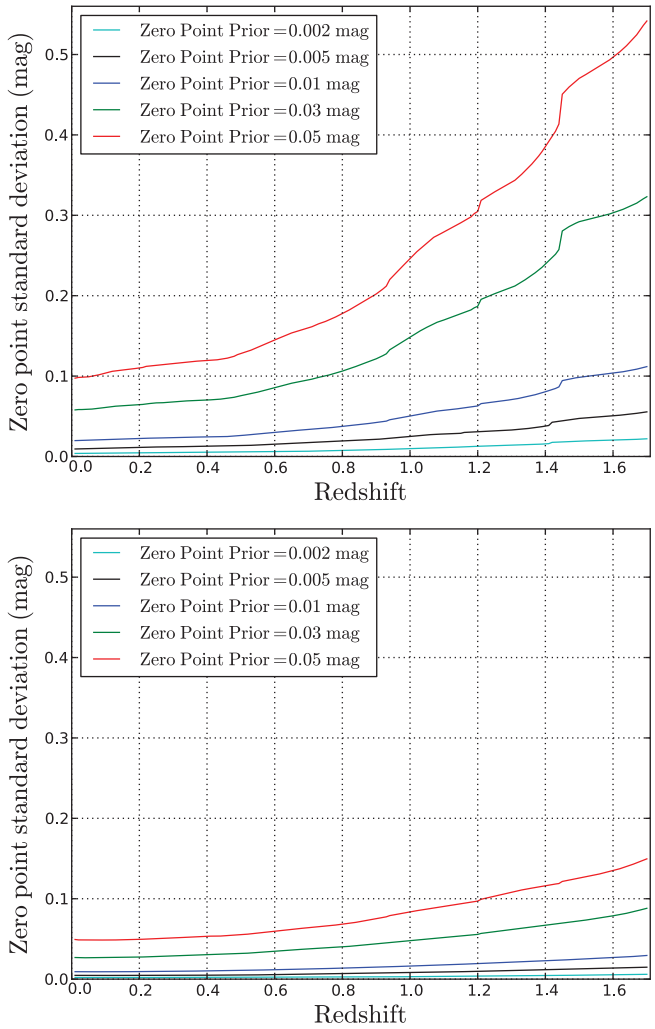

Fig. 1. Zero-point covariance matrices standard deviations σ_a derived from MC, for different values of the zero-point priors, as a function of redshift. Upper panel: fitting for $B_V \equiv A_V/R_V$. Lower panel: fixing $R_V = 3.1$. The two panels have the same scale to show how fitting for B_V significantly increases σ_a.

2.2. Simulating the zero-point uncertainty in the simultaneous fit

The model we adopt to describe our simultaneous μ fit, taken from KM, is the following: for N observed supernovae, with supernova i observed in a set of filters $k = 1,\ldots,N_{\rm F}$, we have:

$$\begin{aligned}
&m_k^1 = \mu^1 + \alpha(S^1 - 1) + M(z_1)_k + A_V^1 a(z_1)_k + B_V^1 b(z_1)_k + \mathcal{Z}_k,\\
&s_k^1 = S^1,\\
&\vdots\\
&m_k^N = \mu^N + \alpha(S^N - 1) + M(z_N)_k + A_V^N a(z_N)_k + B_V^N b(z_N)_k + \mathcal{Z}_k,\\
&s_k^N = S^N,\\
&\mathcal{Z}_k^{\rm obs} = \mathcal{Z}_k.
\end{aligned} \tag{8}$$

The meaning of the symbols that also appear in Eqs. (1) is the same and the effect of the filter zero-point uncertainty is modeled by the set of parameters $\mathcal{Z}_k$, one for each filter. This contrasts with the SN by SN case where the $\mathcal{Z}_k$ are treated as random magnitude shifts chosen from a defined probability distribution and added to the peak magnitudes. $\mathcal{Z}_k^{\rm obs}$ are measured zero-point values and their uncertainty is described by a measurement covariance matrix $V_{\mathcal{Z}}$; in the following we assume $\mathcal{Z}_k^{\rm obs} = 0$ mag. The covariance matrix $V_{\mathcal{Z}}$ may or may not be diagonal; the diagonal case $V_{\mathcal{Z}} = {\rm diag}\,(\sigma_1^2 \cdots \sigma_{N_{\rm F}}^2)$ (for $N_{\rm F}$ filters) amounts of course to assuming that the filter zero-points uncertainty are all uncorrelated. This simple assumption is made in KM and, while it is too simplistic, deriving a more realistic model would require a detailed knowledge of the actual experiment. In our analysis we will not try to do that but will rather consider uncorrelated zero-points (but see Samsing and Linder [24] for an attempt to model the effect of correlated zero-point uncertainties between filters via Principal Component Analysis). In writing down Eqs. (8) we have implicitly assumed that the zero-points do not vary in time and therefore can be represented by a single set of $\mathcal{Z}_k$ parameters. This is a reasonable assumption for the space-based mission we will consider in our simulations, but may not be for other experiments; for example in a ground-based experiment zero-points may be expected to vary with atmospheric conditions. However, even in the case of time-varying zero-points the KM model can still be used; in the ground-based case mentioned above one may introduce separate sets of $\mathcal{Z}_k$ for a set of different atmospheric conditions and assign a set to each supernova depending on these conditions on the date of observation; other cases where this approach can be used are modeling changes in the instrument during a very long mission or combining different experiments.

Eqs. (8) form a linear system of $2\langle N_{\rm Obs}\rangle \times N$ observations and $N_{\rm Par} \equiv 4 \times N + N_{\rm F}$ parameters, where $\langle N_{\rm Obs}\rangle$ is the mean number of observed bands used in the fit per supernova (5 in our simulations), the factor of 2 is there because for each band we have a peak magnitude and a stretch, and the factor of 4 is there because each supernova is described by four parameters μ, S, A_V, B_V in addition to the zero-point parameters $\mathcal{Z}_k$. For a typical stage IV space-based dark energy mission, as defined by the Dark Energy Task Force (DETF: see [1]), this may translate to 22,000 observations and 9000 parameters; fortunately the Fisher matrix of the system of Eqs. (8), whose inversion is the main computational hurdle in implementing the KM model, is very sparse since the only non-zero entries come from 4×4 matrices along its diagonal, corresponding to the supernova parameters, and from the entries whose row or column index correspond to the zero-point parameters that introduce correlations among the supernovae; therefore the total number of non-zero entries scales as N, not N^2; the solution of

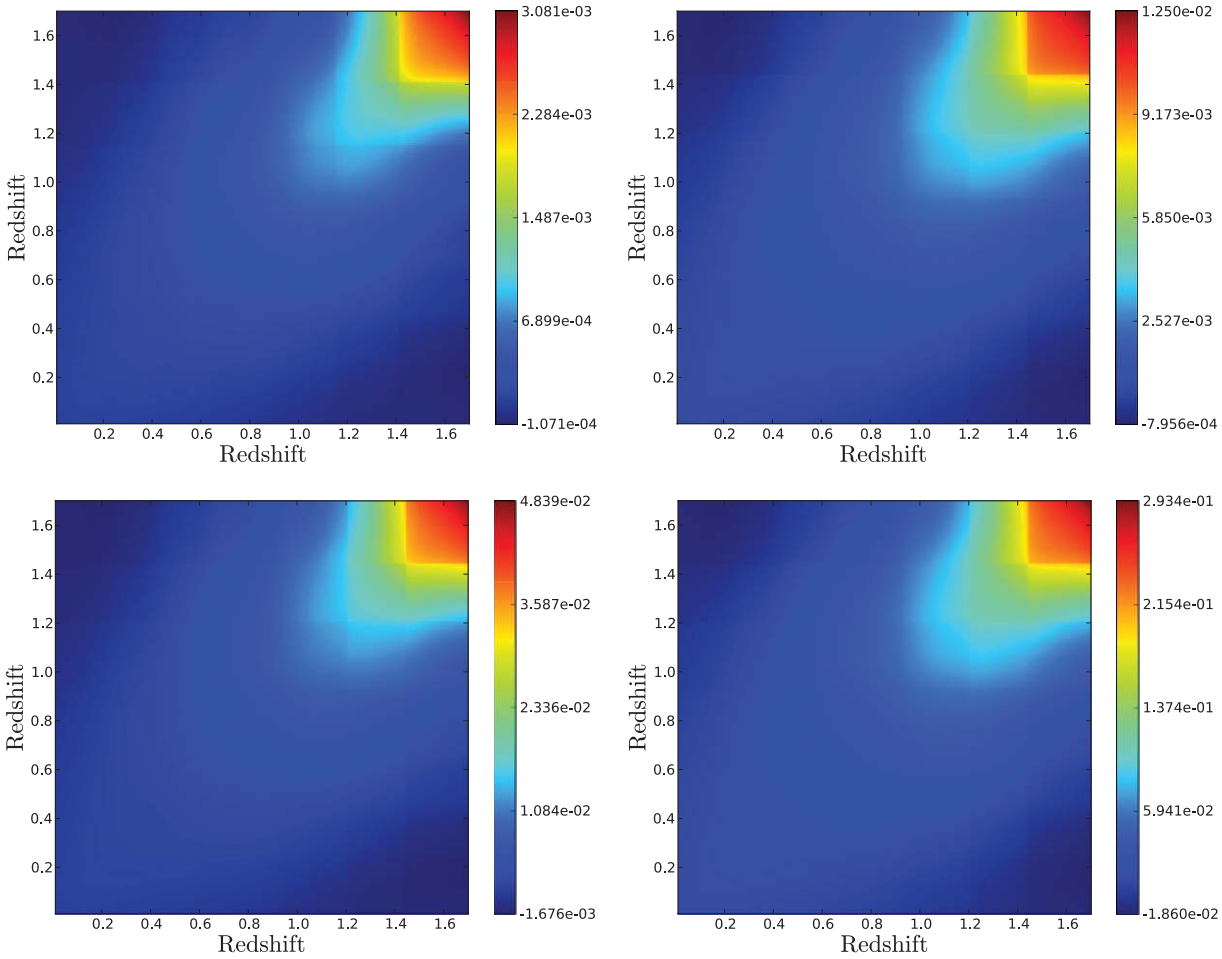

Fig. 2. Color maps of zero-point covariance matrices computed via the MC. Upper left panel: zero-point prior 0.005 mag. Upper right panel: zero-point prior 0.01 mag. Lower left panel: zero-point prior 0.02 mag. Lower right panel: zero-point prior 0.05 mag.

the system of Eqs. (8) can therefore be accomplished in about 1 h on a 3 GHz desktop with 16 GB of memory.

Note that when $V_{\mathcal{Z}} \to 0$ the supernovae in the system of Eqs. (8) become decoupled and the model reduces to the traditional SN by SN fit; the cosmology fit results of the two approaches must then be the same; mathematically the entries in the Fisher matrix whose row or column indices correspond to the zero-point parameters $\mathcal{Z}_k$ become zero and the Fisher matrix itself becomes block diagonal, with a 4×4 non zero block for each supernova.

2.3. Modeling the input data uncertainties

We have so far focused on the zero-point uncertainties, but other sources of uncertainty affect the measured magnitudes in each band. The most important of these are: measurement errors due to Poisson noise (which was approximated as a Gaussian in our simulation tool), a possible color uncertainty, any remaining statistical uncertainty, and any remaining systematic not described by our model.

We model the remaining statistical uncertainties by assuming an intrinsic dispersion $\sigma_{\rm Disp} = 0.1$ mag for each supernova in the dataset after stretch and color correction; this value is consistent with values of intrinsic dispersion used by recent surveys such as ESSENCE [26] and is also used by the DETF [1] for stage IV experiments such as JDEM.

We then include the possibility of an intrinsic color dispersion, which is not modeled by adding the same intrinsic dispersion to each supernova, since this affects each band in the same way. Instead we model an intrinsic color dispersion by adding a new, in principle non-diagonal covariance matrix to the diagonal Poisson measurement covariance matrix before fitting for the model described by Eqs. (8). Therefore we have the following model of input data uncertainties: $V_{\rm SN\ Data} = V_{\rm Poisson} + V_{\delta_c}$. For simplicity we will consider only $V_{\delta_c} = {\rm diag}(\delta_c^2)$ where δ_c is a constant. Note that in spite of its form V_{δ_c} affects supernovae at different z, and therefore observed in a different number of bands, differently: this color uncertainty model contributes to a magnitude uncertainty of $\sim \sqrt{N_{\rm obs}}\delta_c$ for a supernova with $N_{\rm obs}$ measured bands. In our analyses we will consider both $\delta_c = 0$ and $\delta_c \neq 0$.

After performing the linear μ fit described by Eqs. (8s) with $V_{\rm SN\ Data}$ as data covariance matrix, the covariance matrix from the fit, V_μ, is added to the matrix representing the 0.1mag supernova intrinsic dispersion described above, obtaining the matrix $V_{\rm Cosmology\ Fit} = V_\mu + V_{\rm Disp}$, where $V_{\rm Disp} = {\rm diag}(0.1\ {\rm mag})$. This is then used as the data covariance matrix for the cosmology fit described in Section 2.4 below. The cosmology fit is also the place where possible additional systematics are taken into account, by adding an appropriate covariance matrix to $V_{\rm Cosmology\ Fit}$ (see Section 2.4). The SN by SN case is handled slightly differently: for each supernova i, the distance modulus μ^i is derived independently by fitting the model described by Eqs. (1), along with a covariance matrix V_μ^i that does not include the effect of zero-point uncertainties. The uncertainties in μ^i derived from V_μ^i are combined in a single diagonal matrix and zero-point uncertainties are included by adding a non-diagonal matrix obtained by interpolation of the matrix $V_{\rm ZP}$, obtained from the MC, as described in

Table 1
Mission parameters.

Telescope aperture	1.5 m
Exposure time	1200 s in four dithered exposure of 300 s each
Cadence	4 days
Filters	5 in the optical, 3 in the NIR
Observed SNe Ia	2000 with flat z distribution

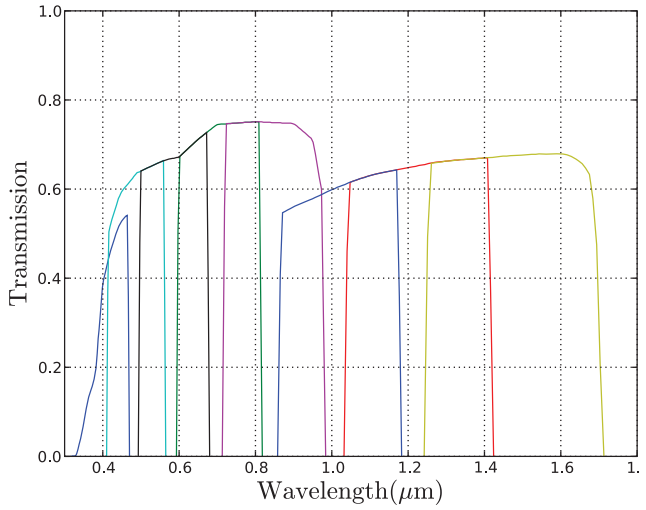

Fig. 3. Channel throughputs for the eight channels (five optical and three NIR) assumed in the simulation; the transmissions refer to the telescope + filter + detector combinations.

Section 2.1; $V_{\rm Disp}$ and possibly other systematics are then included, and the cosmology fit is performed.

2.4. Cosmology fit

We fit to a flat cosmology with Dark Energy Equation of state (EOS) parametrized by $w(a) = w_0 + w_a\ (1-a)$ where $a = 1/(1+z)$ is the scale factor, with a prior on the reduced distance to the last scattering surface ($\tilde{d}_{\rm LSS}$) at $z_{\rm LSS} = 1089$ with a 0.2% fractional uncertainty where:

$$\tilde{d}_{\rm LSS} = \sqrt{\Omega_m h^2}\int_0^{z_{\rm LSS}} \frac{{\rm d}z}{\sqrt{\Omega_m(1+z)^3 + (1-\Omega_m)\exp(3\int_0^z \frac{1+w(z')}{1+z'}{\rm d}z')}}. \quad (9)$$

This gives an excellent representation of the expected Planck CMB constraints for combining with supernova data [16,9].

We chose a fiducial flat ΛCDM cosmology with $\Omega_m = 0.3$, consistent with the value found by Kowalski et al. [14] when fitting for such a cosmology. For presenting our results we use the DETF Figure of Merit (FoM: [1]) as the reciprocal of the square root of the determinant of the covariance matrix after marginalization to w_0, w_a. This now allows us to investigate the effect of zero-point uncertainties in supernova experiments to understand dark energy.

2.5. Mission simulation

While we have so far been quite general in describing our zero-point uncertainty model, we now focus on a specific example of a mission. We choose to simulate a space mission based on the proposed SuperNova Acceleration Probe[5] (SNAP) satellite [25], but with a different configuration than the one described there. The most important differences with the original SNAP proposal concern the telescope aperture, the number of filters, the maximum survey redshift, and the redshift distribution; these choices are based (at the time this paper is written) on what the future JDEM mission may look like. The most important mission parameters we used are reported in Table 1.

We choose a flat z distribution because such distribution was considered by the JDEM Interim Science Working Group for a mission whose light-curve building instrument's field of view was too small for multiplexed observations. In this situation a rolling search is inefficient, instead targeted follow-up allows the mission designers to customize the redshift distribution to be flat.

The throughputs of the eight channels are shown in Fig. 3; these are the transmission of the telescope + filter + detector combinations.

3. Results

We use our simulation tool to explore a larger parameter space than KM. In particular we want to:

1. Compare the two fit methods as a function of zero-point uncertainties for a baseline mission, modeled on the SNAP satellite, with realistic z distributions. We show that the simultaneous fit greatly outperforms the SN by SN fit; therefore we will concentrate on the simultaneous fit in the subsequent analyses.
2. Investigate how the FoM, for the simultaneous fit, varies as mission parameters are changed; in particular we focus on the effects of
   - maximum survey redshift $z_{\rm max}$.
   - number of supernovae observed by the mission, $N_{\rm SN}$.
3. Include additional systematics. We will focus on the systematics model described in Linder and Huterer [15] (hereafter referred to as "LH systematic").

3.1. Making the case for simultaneous fit: results for the baseline mission

We now present the first main result of the paper: fitting for all supernovae at once vastly outperforms the traditional SN by SN fitting, in the sense that the FoM decreases much more slowly with increasing zero-point uncertainties in the simultaneous fit case. We present results for realistic mission parameters and four different values of the color uncertainty δ_c: $\delta_c = 0$, 0.005, 0.01, and

Table 2
FoM of SN by SN fit vs. FoM of simultaneous fit, for color uncertainty $\delta_c = 0$, 0.005, 0.01, and 0.02 mag.

Zero-point uncertainty (mag)	$\delta_c = 0$ mag		$\delta_c = 0.005$ mag		$\delta_c = 0.01$ mag		$\delta_c = 0.02$ mag	
	SN by SN fit	Sim. fit	SN by SN fit	Sim. fit	SN by SN fit	Sim. fit	SN by SN fit	Sim. fit
0	311	311	306	306	295	295	262	262
0.001	246	309	244	302	238	288	217	252
0.002	167	309	166	298	163	283	153	246
0.003	122	308	121	295	120	278	113	239
0.004	95	308	94	292	93	273	88	232
0.005	76	308	76	291	75	268	71	226
0.006	63	308	62	290	61	265	58	219
0.01	35	308	35	288	35	257	33	202
0.02	17	308	17	287	17	252	16	186
0.03	11	308	11	286	10	251	10	181
0.04	7	308	7	286	7	251	7	179
0.05	NC[a]	308	NC[a]	286	NC[a]	250	NC[a]	179

[a] Fit did not converge.

[5] http://snap.lbl.gov.

0.02 mag; the zero-points $\mathcal{Z}_k$ are assumed uncorrelated; we always assume $z_{\max} = 1.5$. Our results are shown in Table 2.

Several things are worth noting in Table 2:

1. In the case of no zero-point uncertainty the two methods give the same result as they must, since in this case they are mathematically equivalent.
2. The simultaneous fit vastly outperforms the traditional SN by SN both for $\delta_c = 0$ and for the more realistic case $\delta_c \neq 0$. This point was already made by KM, but it is reassuring to see that we can confirm their result for a more realistic mission architecture and with a more sophisticated analysis. Therefore the numbers in Table 2 strongly argue for adopting the simultaneous fit as a general analysis method for future supernova surveys.
3. For the not very realistic case of $\delta_c = 0$ mag the FoM for the simultaneous fit is almost flat as the zero-point varies. This is because in this case self-calibration works so well that the 0.1mag intrinsic dispersion dominates the error budget. In the more realistic case of $\delta_c \neq 0$ the simultaneous fit is still superior: the FoM does decline modestly because of the interaction of δ_c with $\mathcal{Z}_k$ each of which affects bands rather than supernovae as a whole.

To gain more insight into the working of this self-calibration mechanism we consider how the final statistical uncertainties on the fit parameters $\mathcal{Z}_k$ are related to the uncertainties on the zero-point priors $\sigma_{\mathcal{Z}}$. Quantitatively we consider the subcovariance matrix of the $\mathcal{Z}$ parameters alone obtained from the μ fit: its determinant $\det(\mathcal{Z})$ is simply the product of the eigenvalues of this submatrix and $\det(\mathcal{Z})^{1/N_F}$, where $N_F = 8$, should give an estimate of the typical statistical uncertainty in the fit parameters $\mathcal{Z}$ *after* the simultaneous μ fit; we call this determinant $\sigma_{\mathcal{Z}\mathrm{Fit}}$ to emphasize this point. We compare $\sigma_{\mathcal{Z}\mathrm{Fit}}$ with the uncertainty on the zero-point prior *before* the fit, $\sigma_{\mathcal{Z}}$, in Fig. 4; the four lines show results for $\delta_c = 0$, 0.005, 0.01, 0.02 mag. The figure shows that for $\delta_c = 0$, $\sigma_{\mathcal{Z}\mathrm{Fit}}$ grows very slowly as a function of $\sigma_{\mathcal{Z}}$: for $\sigma_{\mathcal{Z}} = 0.05$ mag, $\sigma_{\mathcal{Z}\mathrm{Fit}} = 2 \times 10^{-4}$ mag; this explains the almost constant FoM as a function of $\sigma_{\mathcal{Z}}$ for $\delta_c = 0$ mag reported in Table 2. For $\delta_c \neq 0$ $\sigma_{\mathcal{Z}\mathrm{Fit}}$ is higher by a factor of $3-5$ than the $\delta_c = 0$ mag case even at low $\sigma_{\mathcal{Z}}$ and grows more rapidly as $\sigma_{\mathcal{Z}}$ increases, but it is still much smaller than $\sigma_{\mathcal{Z}}$: for example, for $\delta_c = 0.02$ mag, at $\sigma_{\mathcal{Z}} = 0.05$ mag,$\sigma_{\mathcal{Z}\mathrm{Fit}} = 2 \times 10^{-3}$ mag, a factor of 10 higher than the value

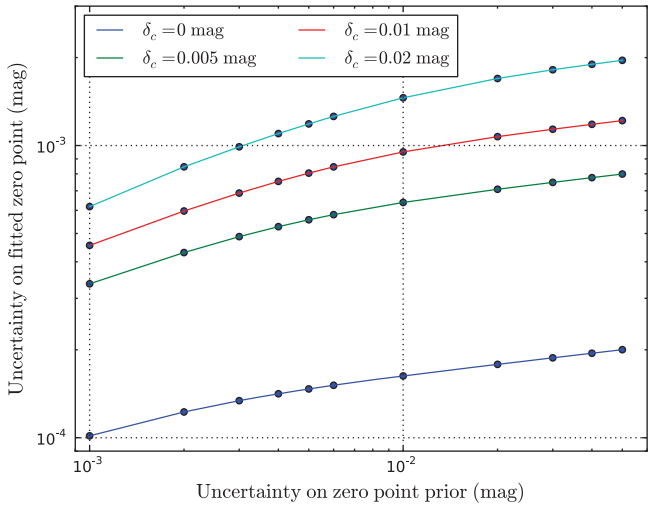

Fig. 4. Typical statistical uncertainty on the zero point parameters $\mathcal{Z}$ after the fit, $\sigma_{\mathcal{Z}\mathrm{Fit}}$, vs. uncertainty on the zero-point prior, $\sigma_{\mathcal{Z}}$, for color uncertainty $\delta_c = 0$, 0.005, 0.01, 0.02 mag.

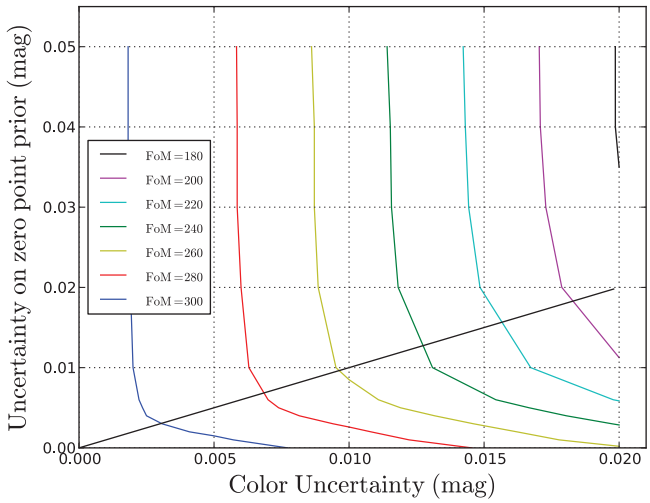

Fig. 5. Contours of constant FoM for different zero-point prior $\sigma_{\mathcal{Z}}$ and color uncertainties δ_c. The straight line at 45° shows the points where zero-point prior and color uncertainty are equal; note that the line intersects the contours roughly where they change their slope from almost vertical ($\sigma_{\mathcal{Z}} > \delta_c$) to almost horizontal ($\sigma_{\mathcal{Z}} < \delta_c$). The case $\sigma_{\mathcal{Z}} > \delta_c$ is the self-calibration regime: the data themselves determine the zero-point more precisely than an accurate zero-point calibration. In the case $\sigma_{\mathcal{Z}} < \delta_c$ a tighter control of zero-point uncertainty is necessary to improve the FoM.

for $\delta_c = 0$ mag, but more than 10 times smaller than $\sigma_{\mathcal{Z}}$. Therefore Fig. 4 shows both why $\delta_c \neq 0$ decreases the FoM as $\sigma_{\mathcal{Z}}$ increases and why the simultaneous fit still outperforms the SN by SN fit.

Because of the large parameter space we are exploring it is convenient to visualize our results as contours of constant FoM as a function of two parameters at the same time. An interesting combination of parameters to consider is given by the zero-point prior $\sigma_{\mathcal{Z}}$ and the color uncertainty δ_c: their relative interplay indicates whether more effort should be expended in calibration or in understanding supernova colors. Fig. 5 shows contours of constant FoM as a function of the uncertainty on the zero-point prior $\sigma_{\mathcal{Z}}$ and the color uncertainty δ_c. The figure shows, not surprisingly, a trade off between these two parameters. What is more interesting is the nearly vertical shape exhibited by the graphs, indicating that it pays off to tightly control the color uncertainty: for example, to achieve a FoM of 240, limiting δ_c to $\lessapprox$0.013 mag results in very lax requirements on the zero-point uncertainty (between 0.01 mag and 0.05 mag), whereas poorer control of the color uncertainty $\delta_c \gtrapprox 0.013$ mag imposes strong requirements on the zero-point ($\lessapprox$0.01 mag); similar considerations hold for other FoMs. Therefore we see the existence of two regimes: the high $\sigma_{\mathcal{Z}}$ regime where tighter control of color uncertainty is more important, and the low $\sigma_{\mathcal{Z}}$ regime, where tighter control of zero-point prior is more important; the transition between these regimes occurs when $\delta_c \quad \sigma_{\mathcal{Z}}$. For $\delta_c < \mathcal{Z}_k$ (high $\sigma_{\mathcal{Z}}$ regime) the decline in the FoM is roughly $60(\delta_c/0.01)$ mag for 0.005 mag $\lessapprox \delta_c \lessapprox$ 0.02 mag and 0.02 mag$\lessapprox\sigma_{\mathcal{Z}}\lessapprox$0.05 mag, so the FoM decline is independent of $\mathcal{Z}_k$ in a 0.03 mag range; in this regime the data themselves determine the zero-point more precisely via self-calibration and tighter control of color uncertainty lead to further improvements whereas tighter zero-point calibration is not essential. When $\sigma_{\mathcal{Z}} < \delta_c$ (low $\sigma_{\mathcal{Z}}$ regime) self-calibration is not dominant and tighter zero-point calibration is necessary to achieve higher FoMs.

This first conclusion for the baseline mission can therefore be drawn from Table 2 and Fig. 5: in order to have an impact above self-calibration alone, filter zero-point uncertainties must be similar to or better than the intrinsic color dispersion.

4. Exploring the mission parameter space

The second aim of this paper is to explore trades in mission design. In this section we wish to explore variations in several parameters from the baseline mission presented in Section 3, analyzing the impact on the results. In particular we focus on two crucial parameters: the maximum survey redshift $z_{\max}$ and the number of observed supernovae $N_{\rm SN}$, while keeping the remaining parameters unchanged; we are particularly interested in different combinations of parameters that give comparable FoMs. This is a particularly interesting combination of mission parameters to consider because spectroscopically following up supernovae at high z is very time consuming since the required time scales as $(1+z)^6$; the parameters in Table 1 remain unchanged but the mission duration varies as $z_{\max}$ and $N_{\rm SN}$ change.

We also wish to consider other sources of systematic uncertainty in addition to zero-point. A much used model of systematic uncertainty in supernova surveys has been presented by Linder and Huterer [15] who introduce a redshift-dependent systematic that models, e.g., a non-standard luminosity evolution or time-varying host-galaxy dust extinction. Their model, which we will refer to as the LH systematic, assigns to each supernova in a bin of central redshift z_b and total width 0.1 an equal share in quadrature of an uncertainty $dm = 0.02(1.7/z_{\max})(1+z_b)/2.7$. Adopting this model, Linder and Huterer [15] show that maximum survey redshifts of $\gtrapprox 1.5$ are necessary to convincingly see evidence of a variation in w. The same model is used by Kim et al. [12] to describe a generic mission systematic, not necessarily due to time-varying host-galaxy extinction. We use the LH systematic in this spirit, namely to describe any other source of systematic not captured by our zero-point uncertainty model, and we repeat the same set of simulations described in this subsection with the LH systematic added. The covariance matrix for the cosmology fit $V_{\rm Cosmology\ Fit}$ is thus given by: $V_{\rm Cosmology\ Fit} = V_\mu + V_{\rm Disp} + V_{\rm LH}$, and the LH systematic is given by:

$$dm = 0.01\,\frac{1+z_b}{2.7} \tag{10}$$

that is, we divide the LH systematic for $z_{\max} = 1.7$ by two since we include calibration uncertainty separately. It is important to note that by adding $V_{\rm LH}$ we are implicitly assuming that the LH systematic is uncorrelated with the other systematics; a more detailed treatment should aim at properly taking into account possible correlations; an example is described by Amanullah et al. [3].

Table 3
FoM as a function of uncertainty on the zero-point prior for five different $z_{\max}$: 1.1, 1.2, 1.3, 1.4, 1.5. Upper panel: the LH systematic not included. Lower panel: the LH systematic included. In all cases $N_{\rm SN} = 2000$ and $\delta_c = 0.01$ mag. The nearby supernova sample is unchanged.

Uncertainty on zero-point prior σ_z (mag)	FoM				
	$z_{\max} = 1.1$	$z_{\max} = 1.2$	$z_{\max} = 1.3$	$z_{\max} = 1.4$	$z_{\max} = 1.5$
0	266	283	290	295	295
0.002	258	273	279	284	283
0.005	245	259	265	269	268
0.010	236	250	255	258	257
0.02	233	246	251	253	252
0.03	232	245	250	252	251
0.04	231	245	249	252	251
0.05	231	244	249	251	250
0	184	201	212	220	225
0.002	180	196	206	214	218
0.005	172	188	197	204	208
0.01	167	182	191	197	201
0.02	165	179	188	194	197
0.03	165	179	188	193	196
0.04	165	179	187	193	196
0.05	164	179	187	193	196

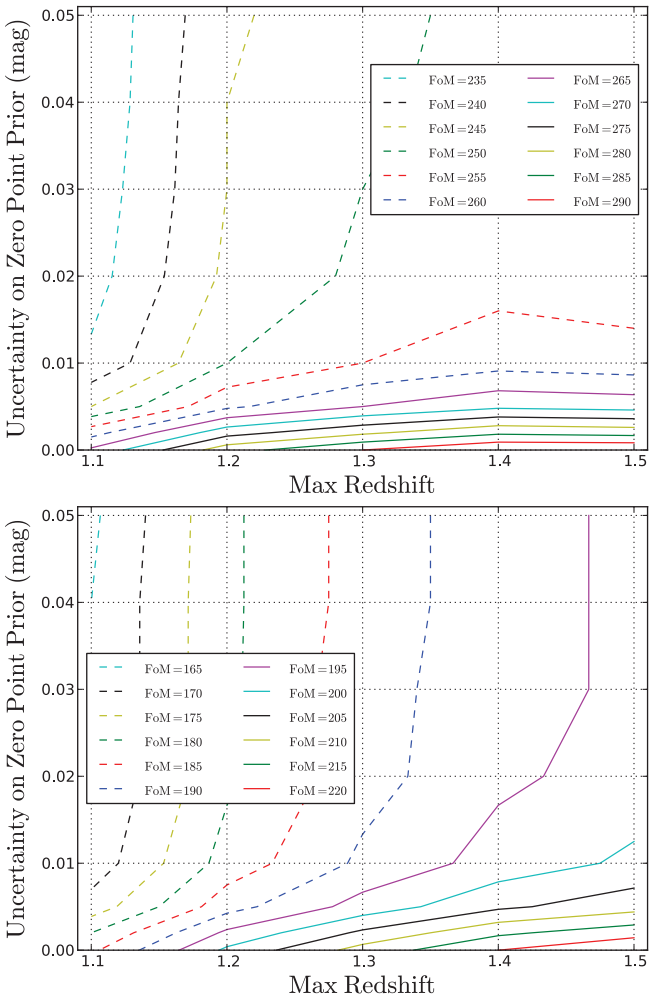

Fig. 6. Contours of constant FoM for different uncertainties on the zero-point prior σ_z and maximum survey redshift $z_{\max}$. We assume $N_{\rm SN} = 2000$ and $\delta_c = 0.01$ mag. Upper panel: the LH systematic is not included. Lower panel: the LH systematic is included.

We now present our results obtained considering the $N_{\rm SN}$, z_{max}, σ_z combination, keeping in turn one of these parameters fixed, and varying the other two. In all cases we will report tables of FoM and contour plots of constant FoM made from these tables; all results will be given with and without the LH systematic. We will also assume in the following $\delta_c = 0.01$ mag. When we keep $N_{\rm SN}$ fixed we choose $N_{\rm SN} = 2000$; when we keep $z_{\max}$ fixed we choose $z_{\max} = 1.5$.

4.1. Influence of maximum survey redshift z_{max}

We consider surveys with $z_{\max} = 1.1$, 1.2, 1.3, 1.4, and 1.5 always keeping the other mission parameters fixed. The results are reported in Table 3 with and without including the LH systematic; contour plots of constant FoM as a function of $z_{\max}$ and σ_z at constant $N_{\rm SN} = 2000$ and $\delta_c = 0.01$ mag are shown in Fig. 6 without including the LH systematic in the upper panel and including it in the lower panel.

The upper panel of Fig. 6 shows the existence of two regimes divided by FoM $\approx$ 250: for FoM $\lessapprox 250$ the contours are almost vertical, whereas for FoM $\gtrapprox 250$ they become almost horizontal. The former is the self-calibration regime, where, as remarked, the data themselves determine the zero-point precisely; however

self-calibration is less effective with increasing redshift because fewer filter observations are used for each supernova as z_{max} increases. The figure suggests that if there is no redshift dependent systematic then not surprisingly z_{max} becomes less important: a FoM = 250 could be achieved for $\sigma_z = 0.05$mag and $z_{max} = 1.3$. For FoM > 250 we are not in the self-calibration regime anymore and to achieve FoMs this high zero-point uncertainties must be tightly controlled ($\sigma_z \lessapprox 0.01$ mag).

The inclusion of the redshift dependent LH systematic however changes the conclusions above as shown in the lower panel of Fig. 6. Apart from the obvious hit in the FoM it introduces (reducing it by 70: clearly the LH systematic is dominant), there is also continuous improvement in FoM with higher z_{max}. As expected, one can trade off σ_z and z_{max}: a FoM 200 can be achieved either by σ_z 0.01 mag and z_{max} 1.5 or σ_z 0.003 mag and z_{max} 1.3. The lower maximum survey redshift, with its reduced spectroscopic time, can achieve similar results *if* much more stringent zero-point requirements can be met.

4.2. Influence of the maximum number of observed supernovae N_{SN}

We consider surveys with $N_{SN} = 1500, 1800, 2000$ while keeping $z_{max} = 1.5$. Table 4 shows our results with and without including the LH systematic. Fig. 7 shows the contour plots made from Table 4 without including the LH systematic in the upper panel and including it in the lower panel.

In the upper panel of Fig. 7 we again see the existence of the two regimes distinguished by FoM 250 we noted in Fig. 6; this shows that the larger the number of supernovae per redshift bin the better the self-calibration can be done. The figure shows that achieving FoM $\gtrapprox$ 250 requires a tight control of zero-point uncertainties $\sigma_z \lessapprox 0.01$ mag, at least if one considers $N_{SN} \leqslant 2000$. (We did not consider $N_{SN} > 2000$ because such numbers would probably be unrealistically high for a future space-based mission). For FoM $\lessapprox$ 250 on the other hand zero-point requirements are much less severe. The existence of these two regimes can once again be explained by self-calibration: for FoM $\lessapprox$ 250 and $\sigma_z \gtrapprox 0.02$ mag we are in the self-calibration regime and the contours are therefore roughly vertical, indicating that the FoM is quite insensitive to the actual value of the zero-point prior σ_z. In this regime it pays to increase N_{SN}; an increase of 10 in FoM can be achieved by observing 150 more supernovae, almost regardless of σ_z. For FoM $\gtrapprox$ 250 and $N_{SN} \leqslant 2000$ we are not in the self-calibration regime anymore and the contours

Table 4
FoM as a function of uncertainty on the zero-point prior for three different N_{SN}: 1500, 1800, 2000. Upper panel: the LH systematic is not included. Lower panel: the LH systematic is included. In all cases $z_{max} = 1.5$ and $\delta_c = 0.01$ mag. The nearby supernova sample is unchanged.

Uncertainty on zero-point prior σ_z (mag)	FoM		
	$N_{SN} = 1500$	$N_{SN} = 1800$	$N_{SN} = 2000$
0	259	282	295
0.002	249	271	283
0.005	235	256	268
0.01	224	245	257
0.02	219	240	252
0.03	217	238	251
0.04	217	238	251
0.05	217	238	250
0	204	218	225
0.002	198	211	218
0.005	188	201	208
0.01	181	194	201
0.02	177	190	197
0.03	176	189	196
0.04	175	189	196
0.05	175	189	196

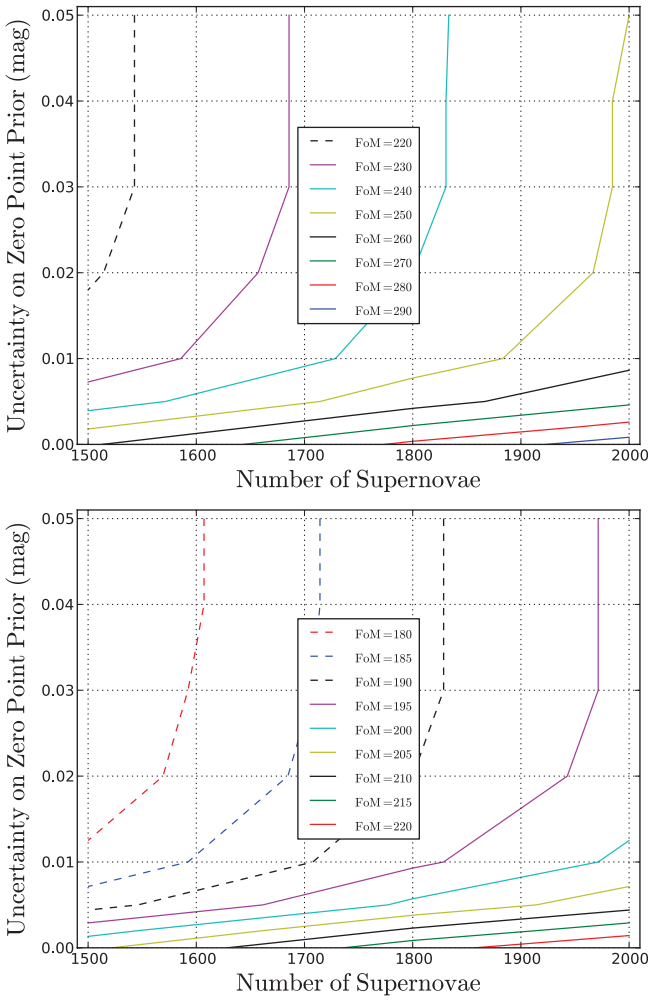

Fig. 7. Contours of constant FoM for different uncertainties on the zero-point prior σ_z and maximum number of supernovae N_{SN}. We assume $z_{max} = 1.5$ and $\delta_c = 0.01$ mag. Upper panel: the LH systematic is not included. Lower panel: the LH systematic is included.

are almost flat: a tighter control of zero-point uncertainties is necessary to achieve higher FoMs. Fig. 7 shows that in this regime an increase of 500 supernovae, from 1500 to 2000 results in only less than 0.01 mag relaxation in the σ_z requirement.

Including the LH systematic does not change this conclusion much: from the lower panel of Fig. 7 we again notice the overall decrease of about 70 in FoM and we see that a tight control of zero-point uncertainties ($\sigma_z \lessapprox 0.01$ mag) is required to achieve FoM $\gtrapprox$ 200. Interestingly, for $\sigma_z \gtrapprox 0.02$ mag, to achieve an increase in FoM 10, additional 220 more supernovae are required (at least if uniformly distributed), compared with 150 without including the LH systematic; this conclusion argues for observing modest numbers of supernovae at high z rather than many at lower z, consistent with the conclusions of Linder and Huterer [15].

4.3. Varying N_{SN} and z_{max} simultaneously

To further investigate the interplay of N_{SN} and z_{max}, we varied them simultaneously while keeping the uncertainty on the zero-point prior σ_z fixed at 0.005 and 0.01 mag. Again the inclusion of LH systematic changes the conclusion in each case.

The results are shown in Table 5; the contour plots drawn from the data in the table are shown in Figs. 8 and 9; the upper panels show results without including the LH systematic, the lower panels

Table 5
FoM as a function of number of supernovae N_{SN} and maximum survey redshift z_{max} for fixed uncertainty on the zero-point prior $\sigma_{\mathcal{Z}} = 0.005, 0.01$ mag. FoMs are reported both with and without including the LH systematic. We assume $\delta_c = 0.01$ mag. The nearby supernova sample is unchanged.

N_{SN}	z_{max}	FoM			
		$\sigma_{\mathcal{Z}} = 0.005$ mag No LH	$\sigma_{\mathcal{Z}} = 0.005$ mag LH	$\sigma_{\mathcal{Z}} = 0.01$ mag No LH	$\sigma_{\mathcal{Z}} = 0.01$ mag LH
1500	1.1	216	159	207	154
1500	1.2	227	171	218	165
1500	1.3	231	179	221	172
1500	1.4	232	183	221	175
1500	1.5	235	188	224	181
1800	1.1	235	168	227	163
1800	1.2	245	180	236	175
1800	1.3	253	191	243	184
1800	1.4	257	198	246	191
1800	1.5	256	201	245	193
2000	1.1	245	172	236	167
2000	1.2	259	188	250	182
2000	1.3	265	197	255	191
2000	1.4	269	204	258	197
2000	1.5	268	208	257	201

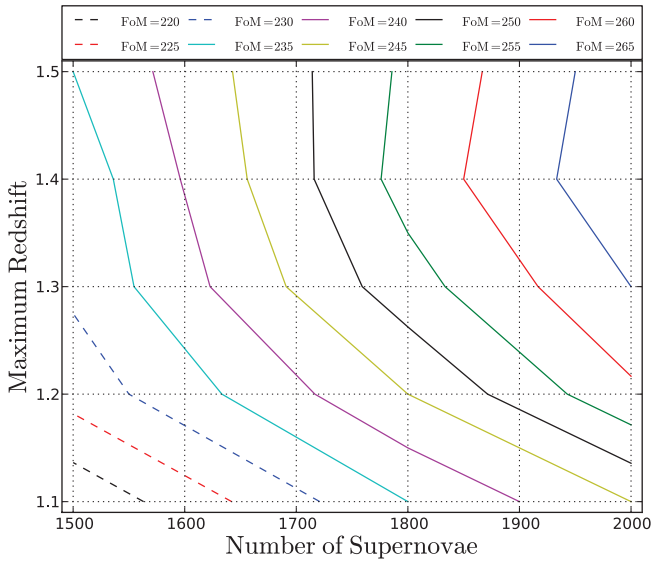

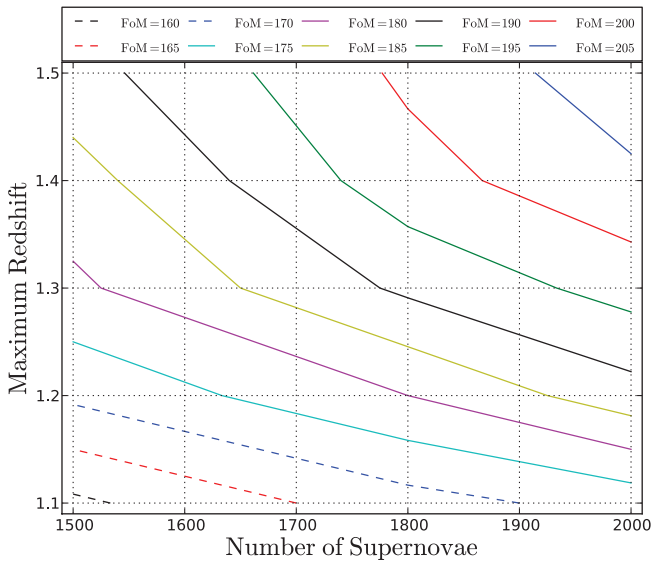

Fig. 8. Contours of constant FoM for different numbers of supernovae N_{SN} and maximum survey redshift z_{max} at fixed zero-point prior uncertainty $\sigma_{\mathcal{Z}} = 0.005$ mag. We assume $\delta_c = 0.01$ mag. Upper panel: the LH systematic is not included. Lower panel: the LH systematic included.

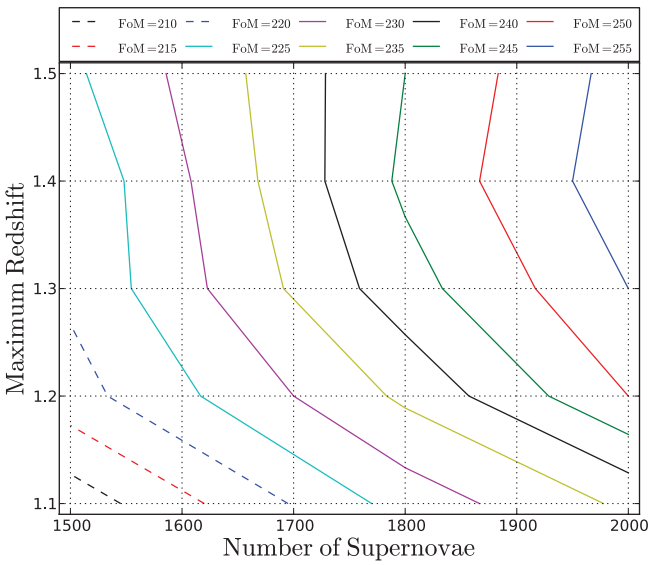

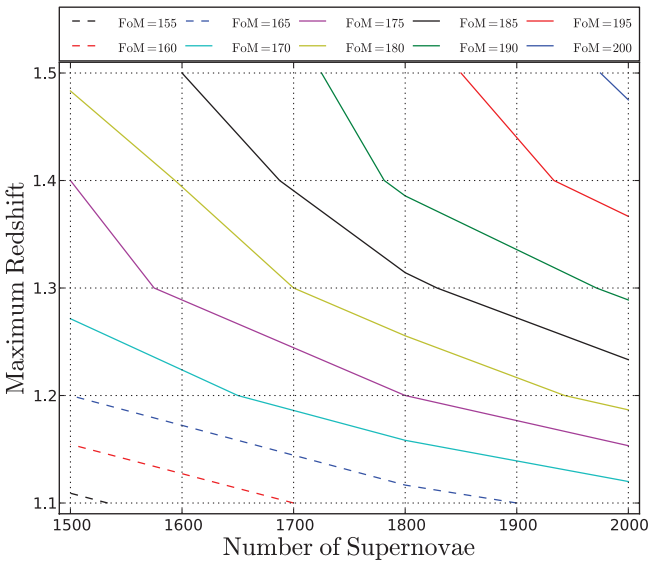

Fig. 9. Contours of constant FoM for different numbers of supernovae N_{SN} and maximum survey redshift z_{max} at fixed zero-point prior uncertainty $\sigma_{\mathcal{Z}} = 0.01$ mag. We assume $\delta_c = 0.01$ mag. Upper panel: the LH systematic not included. Lower panel: the LH systematic included.

including it. Both panels in these figures show, unsurprisingly, a tradeoff between N_{SN} and z_{max}. Without any redshift dependent systematic, for the higher FoMs (FoM $\gtrapprox 250$ for $\sigma_z = 0.005$ mag, FoM $\gtrapprox 245$ for $\sigma_z = 0.01$ mag) going to higher z_{max} is not only ineffective, but even counterproductive: the optimum z_{max} is about 1.4. The inclusion of the LH systematic, shown in the lower panels of the figures, changes this conclusion, showing once again the importance of a high z_{max}: only high z_{max} can achieve high FoM. Only if one is willing to settle for low FoM can one lower z_{max} and compensate by an increase in N_{SN}. We finally note that with the simultaneous fit calibration uncertainties are a subdominant component to LH in the error budget, whereas with the SN by SN fit calibration uncertainties are dominant.

5. Discussion and conclusion

Adopting the general method of modeling zero-point uncertainties introduced by KM we have carried out simulations of a future space-based supernova dark energy experiment with the main aim of assessing the influence of zero-point uncertainties on its overall performance. We have confirmed KM results for a more realistic experiment: fitting for all supernovae at once results in a greatly improved mission performance over the traditional SN by SN fitting. Whereas this effect may not be evident in today's surveys involving a few hundreds of supernovae and few available bands, it will become very significant for future surveys. We explored a representative section of the mission parameter space paying particular attention to how zero-point requirements can be traded off with other mission parameters; in particular we have shown that in general going to higher redshift results in less stringent zero-point requirements, even without considering other form of systematic. We stress once again that, while our results are for a specific possible space-based mission, the KM model itself is more general. The inclusion of a redshift dependent systematic such as the LH systematic greatly affects the mission performance, both by significantly degrading the FoM and by making the case for higher redshift even stronger; it is therefore extremely important to better characterize other forms of systematic by the time future stage IV experiments get under way. Finally the tools used here can realistically simulate future dark energy supernova experiments. The work can be expanded in many ways, all easily implementable in our simulation tool. The most obvious examples are different mission architectures, both ground and space-based, different redshift distributions, further models of systematics. For the zero-point uncertainties one can explore tighter characterization in the optical vs the near infrared and variation with time. The latter may be especially relevant for ground-based surveys. A more detailed treatment of the nearby supernova sample would introduce a separate set of zero-point parameters; again this can be accommodated by the KM model.

Acknowledgements

This work was supported by the Director, Office of Science, Office of High Energy Physics, of the US Department of Energy under Contract No. DE-AC02-05CH11231.

References

[1] A. Albrecht, et al., 2006. Available from: <arXiv:astro-ph/0609591>.
[2] G. Aldering et al., Proc. SPIE 4836 (2002) 61.
[3] R. Amanullah et al., ApJ 716 (2010) 712.
[4] P. Astier et al., A&A 447 (2006) 31.
[5] D. Branch, G.A. Tammann, ARA&A 30 (1992) 359.
[6] J.A. Cardelli, G.C. Clayton, J.S. Mathis, ApJ 345 (1989) 245.
[7] Y. Copin et al., New Astron. Rev. 50 (2006) 436.
[8] K.S. Dawson et al., AJ 138 (2009) 1271.
[9] R. de Putter, O. Zahn, E.V. Linder, Phys. Rev. D 79 (2009) 065033.
[10] M. Hicken, W.M. Wood-Vasey, S. Blondin, P. Challis, S. Jha, P.L. Kelly, A. Rest, R.P. Kirshner, ApJ 700 (2009) 1097.
[11] E.Y. Hsiao, A. Conley, D.A. Howell, M. Sullivan, C.J. Pritchet, R.G. Carlberg, P.E. Nugent, M.M. Phillips, ApJ 663 (2007) 1187.
[12] A.G. Kim, E.V. Linder, R. Miquel, N. Mostek, MNRAS 347 (2004) 909.
[13] A.G. Kim, R. Miquel, Astropart. Phys. 24 (2006) 451.
[14] M. Kowalski et al., ApJ 686 (2008) 749.
[15] E.V. Linder, D. Huterer, Phys. Rev. D 67 (2003) 081303.
[16] E.V. Linder, G. Robbers, J. Cosmol. Astropart. Phys. 6 (2008) 4.
[17] E.V. Linder, Phys. Rev. D 79 (2009) 023509.
[18] J. Nordin, A. Goobar, J. Jönsson, J. Cosmol. Astropart. Phys. 2 (2008) 8.
[19] S. Perlmutter et al., ApJ 483 (1997) 565.
[20] S. Perlmutter et al., ApJ 517 (1999) 565.
[21] S. Perlmutter, B.P. Schmidt, in: Supernovae and Gamma-Ray Bursters, vol. 598, p. 195, 2003. Available from: <arXiv:astro-ph/0303428>.
[22] M.M. Phillips, Stellar candles for the extragalactic distance scale, in: D. Alloin, W. Gieren (Eds.), Lecture Notes in Physics, vol. 635, pp. 175–185.
[23] A.G. Riess et al., AJ 116 (1998) 1009.
[24] J. Samsing, E.V. Linder, Phys. Rev. D 81 (2010) 043533.
[25] SNAP Collaboration: Aldering, G. et al., 2004. Available from: <arXiv:astro-ph/0405232>.
[26] W.M. Wood-Vasey et al., ApJ 666 (2007) 694.